Monthly Notices
of the
ROYAL ASTRONOMICAL SOCIETY

MNRAS **453,** 113–121 (2015) doi:10.1093/mnras/stv1606

Ultrahard spectra of PeV neutrinos from supernovae in compact star clusters

A. M. Bykov,[1,2,3]★ D. C. Ellison,[4] P. E. Gladilin[1] and S. M. Osipov[1]

[1]*Ioffe Physical-Technical Institute of the Russian Academy of Sciences, Saint-Petersburg, 194021, Russian Federation*
[2]*International Space Science Institute, Hallerstrasse 6, CH-3012 Bern, Switzerland*
[3]*Saint-Petersburg State Polytechnical University, Saint-Petersburg, Russia*
[4]*North Carolina State University, Department of Physics, Raleigh, NC 27695-8202, USA*

Accepted 2015 July 14. Received 2015 June 30; in original form 2015 April 29

ABSTRACT

Starburst regions with multiple powerful winds of young massive stars and supernova remnants are favourable sites for high-energy cosmic ray (CR) acceleration. A supernova (SN) shock colliding with a fast wind from a compact cluster of young stars allows the acceleration of protons to energies well above the standard limits of diffusive shock acceleration in an isolated SN. The proton spectrum in such a wind-SN pevatron accelerator is hard with a large flux in the high-energy end of the spectrum producing copious gamma-rays and neutrinos in inelastic nuclear collisions. We argue that SN shocks in the Westerlund 1 cluster in the Milky Way may accelerate protons to $\gtrsim$40 PeV. Once accelerated, these CRs will diffuse into surrounding dense clouds and produce neutrinos with fluxes sufficient to explain a fraction of the events detected by IceCube from the inner Galaxy.

Key words: acceleration of particles – MHD – neutrinos – shock waves – cosmic rays – ISM: supernova remnants.

1 INTRODUCTION

Gamma-ray observations with both space- and ground-based telescopes have shown that supernova remnants are the main sources of cosmic rays (CRs) at least up to 100 TeV. Galactic sources of PeV CRs, however, are still to be identified (e.g. Amato 2014; Blandford, Simeon & Yuan 2014) although it has been argued that Type IIb supernovae, a subclass which comprise about 3 per cent of the observed core collapse SNe, may be able to produce CRs with energies beyond 100 PeV (e.g. Ptuskin, Zirakashvili & Seo 2010). Cosmic neutrino observations are well suited for identifying galactic pevatrons (see e.g. Halzen & Hooper 2002; Aharonian 2004; Becker 2008; Anchordoqui et al. 2014a). The *IceCube South Pole Observatory* (IceCube) has detected 37 neutrino events above the expected atmospheric neutrino background in a 988-d sample (Aartsen et al. 2014a), with three PeV neutrinos, 1.041^{+132}_{-144} PeV, 1.141^{+143}_{-133} PeV and 2.004^{+236}_{-262} PeV, being the most energetic neutrino events in history. While significant spatial or time clustering of the events has not yet been reported, a possible association of some events with galactic centre sources was proposed (e.g. Razzaque 2013).

The ANTARES neutrino telescope (Adrián-Martínez et al. 2014), using six years of data collected near the galactic centre, reported 90 per cent confidence level upper limits on the muon neutrino flux to be between 3.5 and 5.1 $\times$ 10^{-8} GeV cm^{-2} s^{-1}, depending on the exact location of the source. They excluded a single point source as the origin of seven neutrinos observed by IceCube in the vicinity of galactic centre. However, an extended source of a few degrees is not excluded.

Since the most likely high-energy neutrino producing mechanisms are the inelastic p–nuclei and p–γ collisions of protons, where the reaction kinematics result in the energy of the neutrinos to be $\sim$0.05 that of the protons, the energy of the parent protons should exceed 4×10^{16} eV to explain the IceCube observations. The gamma-rays produced in these reactions have $\sim$0.1 of the proton energy (e.g. Halzen 2013). Furthermore, the proton accelerators must be very efficient to produce the high-energy neutrino flux of $\nu F_\nu \approx 10^{-8}$ GeV cm^{-2} s^{-1} sr^{-1} per flavour in the 0.1–1 PeV range detected by IceCube.

Neutrinos from photo-meson $p-\gamma$ interactions in compact particle accelerators, like the cores of active galactic nuclei (AGNs; e.g. Stecker 2013) and gamma-ray bursts (GRBs) (e.g. Waxman & Bahcall 1997; Mészáros & Waxman 2001), along with other models (e.g. Fox, Kashiyama & Mészarós 2013; He et al. 2013; Kashiyama et al. 2013; Murase, Ahlers & Lacki 2013; Ahlers & Murase 2014; Anchordoqui et al. 2014b; Kashiyama & Mészáros 2014; Liu et al. 2014; Tamborra, Ando & Murase 2014), have been proposed to explain the origin of these first-ever IceCube neutrinos.

It has been suggested by Neronov, Semikoz & Tchernin (2014) that IceCube neutrinos and *Fermi*/LAT gamma-rays are both produced in interactions of CRs which have a hard spectrum with a power-law index harder than 2.4 and a cut-off above $\sim$10 PeV. This

★ E-mail: byk@astro.ioffe.ru

assumes the CRs are interacting with the interstellar medium in the Norma arm and/or in the galactic bar.

The role of isolated SNRs in producing PeV CRs is uncertain. The gamma-ray spectra from most shell-type galactic SNRs observed by Cherenkov telescopes show a spectral cutoff well below PeV energies (see e.g. Acero et al. 2015). While future Cherenkov Telescope Array observations may be needed to confirm these results (see e.g. Aharonian 2013), a population of pevatrons is needed to explain the observed spectrum of galactic CRs at and above the spectral knee region. Supernovae with transrelativistic shocks (Budnik et al. 2008; Chakraborti et al. 2011) and Type IIb supernovae (Ptuskin et al. 2010) were proposed to accelerate CRs above PeV energies but the statistics of these potential sources remain to be established. Here, we present a model of a galactic pevatron which produces hard CR spectra with a high efficiency of conversion of SN kinetic energy into the highest energy CRs. We further argue that this PeV CR source has the properties required to explain a number of the IceCube neutrinos detected from the direction of the inner Galaxy.

Core-collapse supernovae in associations of massive OB stars are certain to produce a fraction of galactic CRs, as demonstrated by isotopic measurements by the *Advanced Composition Explorer* (see e.g. Binns et al. 2007). Active star-forming regions may comprise extended associations of massive young stars like Cyg OB2 (see e.g. Wright et al. 2014), as well as compact dense clusters of young massive stars like Westerlund 1 (Wd1). These extended and compact cluster types are distinct in both spatial and temporal scales (e.g. Gieles & Portegies Zwart 2011). Both types of clusters of massive stars are expected to be efficient PeV CR accelerators in starburst and normal galaxies (see Bykov 2014, for a review).

The compact massive cluster Wd1, with an estimated age of 3.5–5 Myr, contains more than 50 post-MS stars (e.g. Clark et al. 2005), including at least 24 Wolf–Rayet (WR) stars of both flavours (representing about 8 per cent of the observed galactic population of WR stars) in about a parsec-scale core (e.g. Clark et al. 2005; Crowther et al. 2006). These massive stars have strong individual winds with an estimated total cluster kinetic power exceeding 10^{38} erg s^{-1}. In the small, dense cluster core these individual winds should combine and drive a fast cluster-scale wind by the mechanisms studied by Chevalier & Clegg (1985) and Stevens & Hartwell (2003). The magnetar CXOU J1647-45, discovered by Muno et al. (2006b) using high-resolution *Chandra* X-ray observations, has been associated with Wd1. This magnetar was likely produced about 10 000 years ago by a supernova with a progenitor star of mass $\geq$40 $M_\odot$ (Muno et al. 2006b; Mereghetti 2008) and remains the only direct evidence of supernova activity in Wd1.

In our pevatron model, an SN blast wave collides with the termination shock of a strong wind generated by the collective action of many massive stars in a compact cluster. Both shocks are assumed to propagate in a homogeneous upstream plasma. We show that proton energies well above a PeV may be produced with a hard spectrum where the CR spectrum at PeV energies is most sensitive to the shock speeds and amplification of magnetic turbulence associated with CR driven instabilities. The model provides a high efficiency of conversion of SN shock–cluster wind ram pressure into PeV CRs which is needed to explain at least some of the IceCube neutrino events. We do not consider an SN interacting with its own wind since individual stellar winds will be unimportant in the compact cluster environment where dozens of massive stars are located within a few parsecs and the wind cavity is smoothed out on this scale.

We show that diffusive shock acceleration (DSA) in systems with colliding shock flows (CSFs) can provide maximum particle energies, CR fluxes, and energy conversion efficiencies well above those produced in an isolated SNR shock of the same velocity (Bykov, Gladilin & Osipov 2013). While CSFs are expected to occur in colliding stellar winds, the most powerful events should happen when an SN shock impacts the extended fast wind of a nearby young massive star cluster.

The important features of shock acceleration in CSFs are: (i) the production of a piece-wise power-law particle distribution with a very hard spectrum of confined particles at the high-energy end just before a break, and (ii) an increase in the maximum energy of the accelerated particles, and the acceleration efficiency, compared to that obtained with DSA at an isolated SNR shock of the same speed. These two properties imply that a substantial fraction of the flow ram pressure is converted into relativistic particle pressure. The high-energy CRs, therefore, must modify the dynamics of the CSF system. To model the spectra of accelerated particles in CSFs, a non-linear, time-dependent model was constructed in Bykov et al. (2013). The maximum energy and absolute fluxes of the accelerated particles, both inside the CSFs, and those escaping the acceleration site, depend on the shock velocities, the number densities, and the magnetic fields in the flows. We show below that sub-PeV and PeV neutrinos from colliding shocks in galactic and extragalactic compact clusters of young stars with reasonable parameters, such as those expected in the Wd1 compact cluster, can explain a fraction of the IceCube neutrino events.

2 PARTICLE ACCELERATION IN COLLIDING SHOCK FLOWS

In order to model the proton acceleration in a compact stellar cluster, we used the non-linear, time-dependent model of CSFs presented in Bykov et al. (2013). The main modification is that here we allow for different parameters for the wind termination shock and the SNR blast wave. We have also introduced an approximation to account for the shape of the shock (as illustrated in Fig. 1) using an analytic expression by Wilkin (1996). Other approximations, such as the Bohm diffusion in the shock vicinity, and a parametrization of the magnetic field amplification (MFA) due to CR-driven instabilities, are the same as in Bykov et al. (2013). The reader is referred to

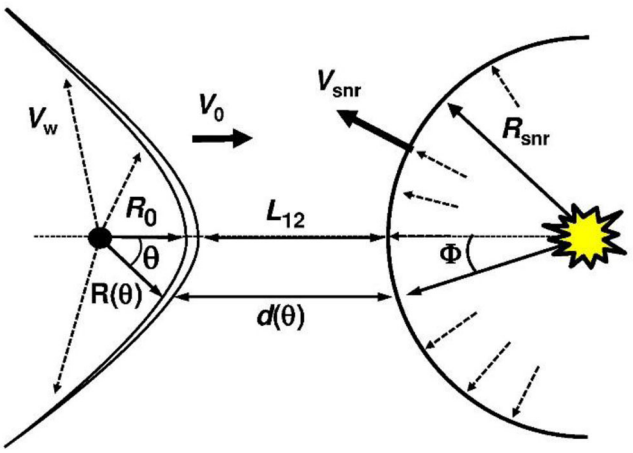

Figure 1. Colliding flow geometry where the stellar wind (left) was approximated from the analytic model of Wilkin (1996), while the SNR shock was assumed to be spherical. The star, or cluster centre, approaches the SN explosion centre with speed V_0. The spectrum of the *Fermi* accelerated CRs was derived taking into account effects of the flow velocity projection on the curved shock surfaces.

that paper for full details. Our results for neutrino and gamma-ray production in Wd1, given in Section 3, use our non-linear, time-dependent model. However, to describe the general characteristics of CSFs, we shall start in this section with simple analytic estimates from a linear model in a plain-parallel case (e.g. Bykov, Gladilin & Osipov 2011).

Considering an SNR expanding in a compact OB-association; at some expansion phase the distance L between the SNR blast wave and a stellar wind shock is less than the mean free path of the highest energy CRs in the SNR shock precursor. At this point, the CR distribution function around the two shocks, indicated by $i = 1$, 2, can be approximated as

$$f_i\,(x,\,p,\,t) = A p^{-3} \exp\left(-\frac{u_i}{D_i}\,|x|\right) \times H\,(p - p_0)\,H\,(t - t_{\rm acc})\,, \quad (1)$$

where the CR acceleration time is

$$t_{\rm acc} = \int_{p_0}^{p} \frac{3}{(u_1 + u_2)}\left(\frac{D_1}{u_1} + \frac{D_2}{u_2}\right)\frac{{\rm d}p}{p}. \quad (2)$$

It is important to note that, besides only applying to high-energy particles with mean free paths larger than L, these equations are qualitatively different from those of test-particle DSA in an isolated shock: the spectrum f_i below the exponential break is harder and the acceleration time is shorter.

Our model assumes a high level of CR-driven magnetic instabilities and Bohm diffusion for CRs in the close vicinity of the shocks (see e.g. Bell 2004; Schure et al. 2012; Bykov et al. 2014). However, once high-energy particles obtain mean free paths of the order or larger than the distance between the shocks, L, scattering will become much weaker. A specific feature of the simulation is that the highest energy CRs, with $p_{\rm max} \geq p \gtrsim p_\star$, propagate with little scattering. Despite the weak scattering between the shocks, their momenta are still nearly isotropic since they scatter for long periods in the extended regions downstream from the shocks. Here, $p_\star$ is the momentum such that the proton mean free path $\Lambda(p_\star) \gtrsim L$. Since the particle distributions are nearly isotropic even for high-energy particles with $\Lambda(p) \gtrsim L$, the kinetic equation reduces to the so-called telegrapher equation (e.g. Earl 1974) and this allows a smooth transition between the diffusive and the scatter-free propagation regimes.

The time-dependent nature of our simulation means that protons escape the accelerator at different stages of the system evolution (i.e. as the SNR blast wave approaches the stellar wind termination shock) producing pions and neutrinos with varying hardness and maximum energy and these effects are included in our results. Of course, the complex evolution of the source and some unknown details of the mass distribution in the outer ISM region (e.g. the presence of dense shells or clouds) will also influence the results. However, we believe the general properties of our simulation are robust.

Assuming Bohm diffusion with $D_1(p) = D_2(p) = D(p) = cR_g(p)/3$, due to CR-driven, amplified magnetic instabilities in the CR accelerator, one obtains

$$t_{\rm acc} \approx \frac{cR_g(p)}{u_{\rm s}\,u_{\rm w}}, \quad (3)$$

where $u_1 = u_{\rm s}$ is the SNR shock velocity, $u_2 = u_{\rm w}$ is the stellar wind speed, and $R_{\rm g}(p)$ is the momentum dependent proton gyroradius. Then, using the scaling $B \approx \sqrt{4\pi\eta_b\rho}\,u_1$ for the amplified magnetic field, the acceleration time can be estimated as $t_{\rm acc} \approx 2 \times 10^{10}\,\epsilon_{\rm PeV}\,(\eta_b n)^{-0.5}\,u_{\rm s3}^{-2}\,u_{\rm w3}^{-1}$ s. In the above expressions, $\rho = m_p n$, η_b is the acceleration efficiency, i.e. the fraction of ram kinetic energy in the plasma flows converted into accelerated particles, the energy is in PeV, and the speeds are in units of 10^3 km s^{-1}.

While the ejecta speed in the free expansion SNR phase can have a wide range of values, we use a mean ejecta speed of $\sim 10^4 (M/{\rm M}_\odot)^{-1/2} E_{51}^{1/2}$ km s^{-1} and take the mean duration of the free expansion phase to be $\sim 200 (M/{\rm M}_\odot)^{5/6} n^{-1/2} E_{51}^{-1/2}$ yr. In the specific case of a young SN shock propagating through the winds of massive stars in the compact cluster Wd1, where $n \sim 0.6$ cm^{-3} (see Muno et al. 2006b), and assuming $\eta_b \sim 0.1$, we find $t_{\rm acc} \approx 400$ yr for a proton accelerated to $\epsilon_{\rm PeV} \sim 40$, when $u_{\rm s3} \sim 10$ and $u_{\rm w3} \sim 3$. The high SN shock velocity $u_{\rm s3} \sim 10$ is expected in the free expansion stage if the fast ejecta mass is about one solar mass.

Therefore, for SNRs with ages less than $t_{\rm SNR} \sim 400$ yr, one can get $t_{\rm acc} < t_{\rm SNR}$ for 40 PeV protons with standard parameters. In this case, at $t_{\rm SNR} \sim 400$ yr, the SNR radius is ~3–4 pc. Furthermore, the hard spectrum expected from CSFs puts most of the energy into the highest energy protons and one can estimate the power in the highest energy neutrinos produced in inelastic p–p-collisions by the decay of charged pions ($\pi^\pm \to e\nu_e\,\nu_\mu\,\bar{\nu}_\mu$) as

$$L_\nu \approx 8 \times 10^{33}\left(\frac{f_\nu}{0.15}\right)\left(\frac{\eta_p}{0.1}\right)\left(\frac{n}{1\ {\rm cm}^{-3}}\right)^2 \times \left(\frac{S}{10^{38}\ {\rm cm}^2}\right)\left(\frac{u_s}{5000\ {\rm km\,s}^{-1}}\right)^3\left(\frac{\tau_c}{10^{10}\ {\rm s}}\right)\ {\rm erg\ s}^{-1}, \quad (4)$$

where f_ν is the fraction of energy in the inelastic p–p–collisions which is deposited in the high-energy neutrinos, S is the cross-section of the colliding flows, and τ_c is the confinement time for protons in the emission region where the target density is $r_{\rm s} \geq 4$ times the ambient density n due to the shock compression, $r_{\rm s}$.

In equation (4), we take the inelastic p–p collision cross-section to be ~70 mb above a proton energy of 10 PeV. Then the proton cooling time, $n\,t_{\rm pp}$, can be estimated as $n\,t_{\rm pp} \approx 2.5 \cdot 10^{14}$ s assuming that two inelastic collisions are needed to convert most of the proton energy into secondaries. The fraction of the proton energy deposited into neutrinos of all types, $f_\nu \sim 0.15$, was derived using both the analytical parameterizations for the inelastic p–p-collisions presented by Kelner, Aharonian & Bugayov (2006), Kafexhiu et al. (2014) and the GEANT4 package simulations. At the energies of photons and neutrinos considered in section 3 the neutrino fluxes calculated with the Kelner et al. (2006) or Kafexhiu et al. (2014) cross-sections differ by less than 20 per cent.

We note that the observed CR energy density and the galactic SN statistics require that $\eta_p \gtrsim 10$ per cent over the lifetimes of isolated SNRs to power galactic CRs. However, the instantaneous efficiency may be much larger during early stages of the SNR evolution (Blasi 2013). In the case of an SNR colliding with a wind, we expect the efficiency to be even higher than in a young isolated SNR and assume it can reach $\eta_p \gtrsim 0.5$ for the CSF stage lasting for a few hundred years (Bykov et al. 2013). Furthermore, since CSFs produce very hard spectra when $t_{\rm acc} \ll t_{\rm esc}$, i.e. $N(\gamma) \propto \gamma^{-1}$, most of the CR energy lies in the high-energy tail just below the upper break which occurs when $t_{\rm acc}$ is greater than the escape time, $t_{\rm esc}$. The essential properties of CSF acceleration in young stellar clusters are high overall acceleration efficiency, spectra harder than $N(\gamma) \propto \gamma^{-2}$, and maximum proton energies $\gtrsim$40 PeV achieved in a few hundred years.

2.1 Colliding flows and 3D geometry effects

While an exact treatment of non-linear CSF with a significant back-reaction from accelerated CRs is unfeasible in 3D, we have introduced an approximation to account for effects from 3D geometry in our plane-parallel model. Instead of taking the cluster wind termination shock and the SNR blast wave as plane, we account for aspects of the curved shock surfaces at positions parametrized by the angles θ or ϕ in Fig. 1. We still assume planar shocks for the DSA calculation but with varying projected velocities at distances $d(\theta) > L_{12}$ along the shock surfaces away from the symmetry axis. Here, L_{12} is the time-dependent minimum distance between the colliding shocks. For each position determined by $d(\theta)$ for $0 < \theta < 90^0$ we calculate the non-linear particle distribution using the projected speeds $V_w \cos\theta$ and $V_{\rm snr} \cos\Phi$ as parallel flow speeds. That is, we assume the wind and the SNR shocks are locally plane with converging parallel flows set by the projected speeds.

For this approximation, we use the bow shock wind model of Wilkin (1996) for $R(\theta)$ and V_w, assume the SNR shock is spherical, and restrict our calculations to 3 arc surfaces: 0°–30°, 30°–60°, 60°–90° which produce accelerated particle densities with the weights 0.84, 0.15 and 0.01, respectively. Then the weighted CR distribution function is used to calculate the gamma-ray and neutrino emissivities both in the accelerator (see Section 3.1) and in the surrounding ISM from the CRs escaped the accelerator (see Section 3.2).

3 NEUTRINOS AND GAMMA RAYS FROM THE WESTERLUND 1 CLUSTER

3.1 Emission from trapped CRs

To explain the IceCube neutrinos, we combine the non-linear, time-dependent model of particle acceleration in CSFs with a propagation model applied to the Wd1 compact cluster (Fig. 2). The time-dependent simulations provide the evolving energy spectra of CR protons and electrons as the SNR shock approaches the strong wind of a nearby early-type star. For relativistic electrons/positrons we account for the energy losses due to synchrotron and IC radiation.

The particle acceleration is combined with a propagation model relevant to Wd1. As described in Section 2, high-energy particles will obtain a hard spectrum when their mean free path is large enough so they scatter back and forth between the two converging shocks. Lower energy particles however, will be confined to, and accelerated by a single shock and obtain a softer spectrum. This phenomenon is illustrated in fig. 3 of Bykov et al. (2013).

It is important to note that even though the CSF acceleration is efficient and the CR population modifies the structure of the plasma flows, the spectrum of high-energy CRs scattering between the two shocks remains hard until they gain enough energy to escape from the system. The shock modification can cause $t_{\rm acc}$ to increase, and the energy where the exponential turnover in equation (1) starts to dominate drop, but below the turnover, the spectrum remains close to $N(\gamma) \propto \gamma^{-1}$.

Thus, the CSF system will have two spectral regimes for trapped CRs: a low-energy region ($\lesssim$1 TeV) from particles accelerated in a single SNR shock (produced both before and after the start of the two-shock acceleration period), and a high-energy, hard spectrum region ($\gtrsim$1 TeV) from particles accelerated in the converging flows. The transition between these two regimes of acceleration occurs when the energy of a particle, E_T, is large enough so it can easily travel between the two shocks.

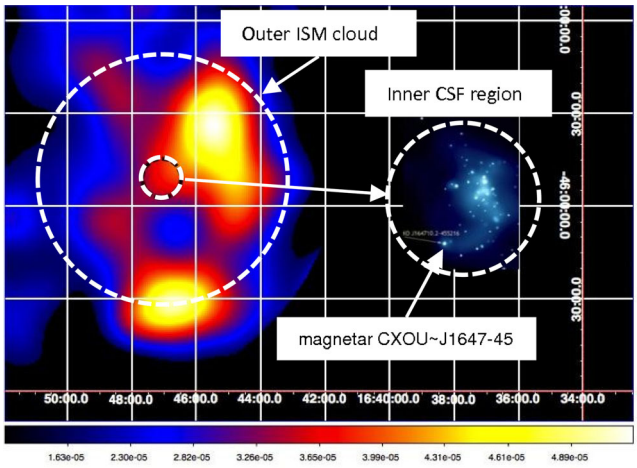

Figure 2. The small dashed circles (not to scale) indicate the inner CR acceleration region in the massive young cluster Wd1. The inner CR acceleration region has a radius of 3–4 pc (shown in a *Chandra* image) and the blow-up of the inner region shows the position of the magnetar CXOU J1647-45 found by Muno et al. (2006b) with a high angular resolution *Chandra* observation of Wd1. The outer region is 30-40 pc centred around Wd1 and indicated by the large dashed circle. This is overlaid on a H.E.S.S. map of TeV emission adapted from Abramowski et al. (2012a). The angular resolution of IceCube is larger than the outer circle. In Fig. 6, we show the larger neutrino emitting ISM volume of radius ∼140 pc around Wd1. The volume is filled over $\sim 10^4$ yr with CRs accelerated during a short CR acceleration phase ∼400 years right after the supernova explosion in Wd1 which produced the magnetar. (See the electronic edition of the Journal for a color version of this figure.)

This transition, occurring at ∼20 TeV, is seen as a bend in the neutrino spectrum shown in Fig. 3. This figure shows neutrinos (solid curve) and gamma-rays (dashed curve) from *p*–*p*-decay from CR protons that are still trapped near the SNR and stellar wind, along with IC from trapped CR electrons. This is the emission expected ∼400 yr after the SN explosion in a region of radius ∼3–4 pc. Note that the gamma-ray fluxes of the sources in Fig. 3 are presented in erg cm^{-2} s^{-1} sr^{-1} in order to be compared with the observed diffuse neutrino fluxes, while the fluxes of the sources in Fig. 4 are measured in erg cm^{-2} s^{-1} as usual.

In Fig. 2, we have overlaid a schematic of this inner CSF region on a map of Wd1. At later times, these 'trapped' CRs will escape the accelerator and diffuse beyond the inner CSF region into a much larger outer ISM region where they may encounter dense clouds producing neutrinos and gamma-rays for an extended period of time, as we discuss in Section 3.2. For clarity, the regions are not drawn to scale in Fig. 2.

To derive the gamma-emissivity of PeV CRs we accounted for the Breit–Wheeler effect of pair production by energetic photons interacting with the interstellar radiation field as well as the extragalactic light background (see e.g. Aharonian 2004; Dwek & Krennrich 2013). This interaction leads to a significant suppression of the gamma-ray flux at the high-energy end of the spectrum for distant (≥10 kpc) sources.

For the emission from Wd1, with an estimated distance of ∼4 kpc, this effect leads to a relatively small suppression of the gamma-ray flux at 1–10 PeV, as can be seen in Figs 3 and 4. In addition to the gamma-rays produced by pion decay, we have also included gamma-rays produced by the IC radiation of the secondary $e^{\pm}$ pairs produced *in situ* by the same *p*–*p*-interactions (see the IC curve in Fig. 4). In this calculation, we accounted for the pair energy losses

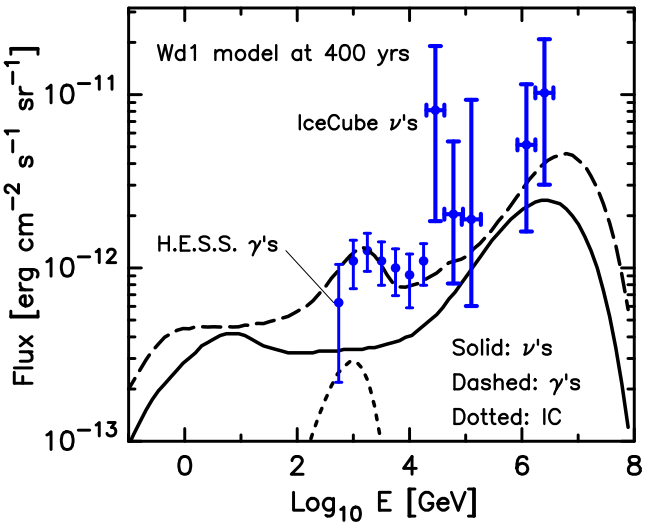

Figure 3. Model predictions of gamma-rays (solid curves) and neutrinos (dashed curves) from p–p-interactions calculated in a CSF source of age 400 yr. The dotted curve is the inverse Compton (IC) emission from primary and secondary electrons accelerated directly in this source. The extreme upward curvature in the neutrino spectrum above ∼10 TeV reflects the transition from CR acceleration in the single SNR shock for low-energy particles to the more efficient acceleration for high-energy particles as they scatter back and forth between the SNR shock and the cluster wind. The data points for the H.E.S.S. source, and the five IceCube events explained in Fig. 5, are presented to illustrate how they compare to our model predictions when the source is ∼400 yr old and point-like, i.e. Wd1 about 10^4 yr ago. The simulated gamma-ray and neutrino emission at the present time from CRs that escaped the accelerator in Wd1 $\sim 10^4$ yr ago are summarized in Figs 4 and 5.

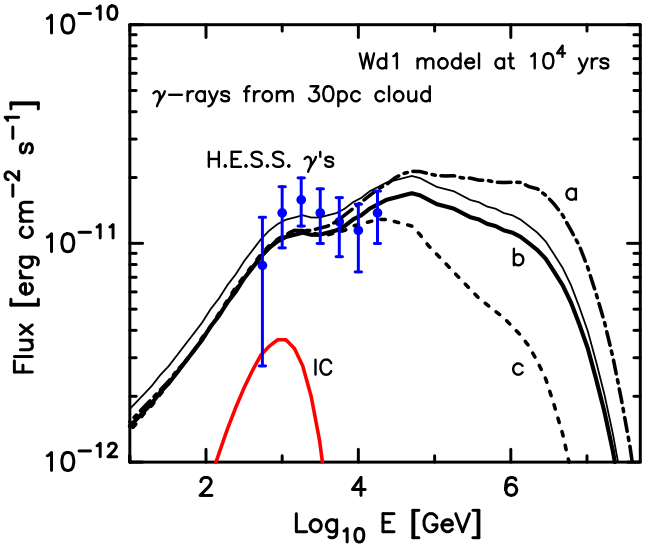

Figure 4. Gamma-ray emission from inelastic p–p-interactions in the CSF source at $\sim 10^4$ yr after the SN explosion when CR protons produced in the short-lived accelerator have propagated into a nearby cloud of ∼30 pc size. The magnetic field amplified by the CR-driven instabilities in the vicinity of the fast shock in the CSF accelerator were parametrized as 0.8 mG (c), 0.9 mG (b), and 1 mG (a), all below 10 per cent of the ram pressure. The IC curve is IC emission from the secondary electrons produced by the inelastic p–p-interactions in the cloud. Only the gamma-rays from the H.E.S.S. field of view are included. The gas number density of the nearby cloud is 25 cm^{-3}, except for the light-weight solid curve where it is 30 cm^{-3} with $B = 0.9$ mG.

in a mean magnetic field of magnitude 10 μG in the extended cloud of number density 25 cm^{-3} (see e.g. Strong, Dickinson & Murphy 2014).

3.2 Emission from escaping CRs

The initial acceleration stage lasts a few hundred years after the SN explosion producing high-energy CRs that escape the CSF system and diffuse through the ambient ISM. However, the estimated age of the supernova which produced the magnetar CXOU J1647-45 in Wd1 is $\sim 10^4$ yr (Muno et al. 2006a; Mereghetti 2008). If the CSF acceleration occurred $\sim 10^4$ yr ago, these CRs will have produced pions over a much longer time span as the TeV–PeV particles diffuse away, fill a region of about 140 pc radius, and interact with the ambient ISM (the outer ISM region indicated in Fig. 2 is about 30 pc).

In Figs 4 and 5, we show simulated gamma-ray and neutrino spectra produced by the CRs that escaped from the accelerator and diffused into the surrounding cloudy medium over 10^4 yr. At this point the acceleration responsible for the emission in Fig. 3 has ceased long ago.

The diffusion model used to propagate the CRs has three regions. Within the accelerator of 3-4 pc radius we assume a Bohm diffusion coefficient $D_{\rm B} = 3 \times 10^{27} E_{\rm PeV}$ cm^2 s^{-1}.

Outside of the dense cloud region we use an ISM value $D_{\rm B} = 3 \times 10^{29} E_{\rm PeV}^{0.33}$ cm^2 s^{-1}, which is consistent with the standard models of CR propagation in the Galaxy (see e.g. Strong, Moskalenko & Ptuskin 2007). Between these two regions we assume a transition coefficient $D_{\rm tran} = D_{\rm B}(R/3\,{\rm pc})^2$, where R is the

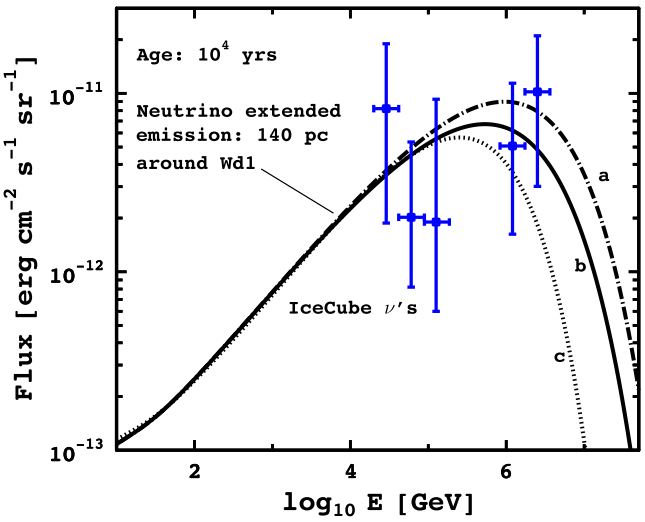

Figure 5. Neutrino emission from an extended (∼140 pc radius) source $\sim 10^4$ yr after the SN explosion when CRs produced in the short-lived accelerator have propagated into the surrounding material. The amplified magnetic fields are 0.8 mG (c), 0.9 mG (b), and 1 mG (a). We note that the gamma-rays in Fig. 4 and the neutrinos here originate from different volumes: only the gamma-rays from the H.E.S.S. field of view are shown in Fig. 4, while the neutrinos are from a larger region of radius 140 pc. The neutrino data points (1σ energy flux error bars) are a subset from all 37 IceCube events (Aartsen et al. 2014a). These five events are within 2σ contours from Wd1 based on Fig. 6. Two PeV events (14, 'Bert') and 35 ('Big Bird'), as well as three sub-PeV (2, 15, 25) events, are included in the subset. Note that the sub-PeV event 25 has a very large position uncertainty in Fig. 6 and have to be considered with some care.

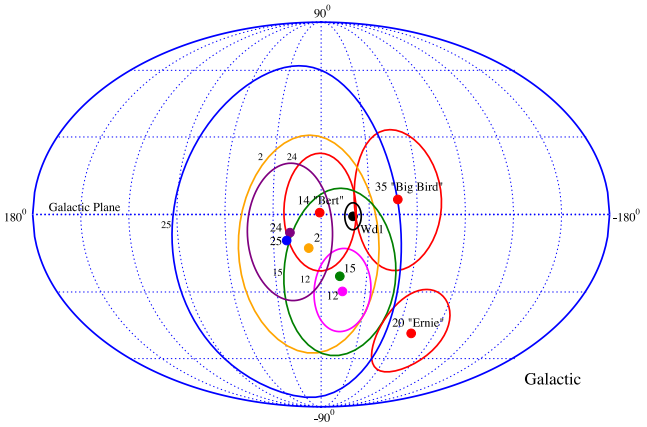

Figure 6. Map showing 2σ contours for a subset of IceCube events associated with the inner Galaxy as determined from 2D Gaussian statistics and the median angular errors and positions given by Aartsen et al. (2014b). Two PeV events (14, 'Bert') and 35 ('Big Bird') as well as three sub-PeV (2, 15, 25) events are within 2σ from Wd1. (See the electronic edition of the Journal for a color version of this figure.)

distance from the core. We assume a mean cloud density $\sim$25 cm^{-3}, cloud radius $\sim$30 pc, and have set, at 1 PeV, $D_{\rm B} = D_{\rm ISM}$ at $R = 30$ pc. A cloud of radius 30 pc with mean density 25 cm^{-3} would have a mass $\sim 10^5$ M$_\odot$. Outside the cloud we assumed an ISM density of $\sim$1 cm^{-3}. We note that the densities we assume for the clouds match available gamma-ray observations of Wd1 (Abramowski et al. 2012a; Ohm, Hinton & White 2013).

The IceCube data points in Fig. 5 show the neutrino energy flux consistent with the position of Wd1 considering the angular resolution of the instrument. The CSF model applied to Wd1 with reasonable parameters can explain a subset of the observed IceCube neutrinos.

4 NEUTRINO PEV AND SUB-PEV EVENTS

The median angular error values for the IceCube neutrino events are given in the Supplementary Material for Aartsen et al. (2014a). Using these median angular errors, and assuming Gaussian statistics (see Aartsen et al. 2014b), we have produced a sky map with 2σ contours (corresponding to about 86 per cent confidence in 2D Gaussian statistics) for the neutrino events in the vicinity of Wd1 (see Fig. 6). As seen in this map, a source of neutrinos with a radius of $\sim$140 pc around Wd1 (black circle) can be associated with five neutrino events, including two PeV events. These are 2, 14 (PeV event 'Bert'), 15, 25 and 35 (PeV event 'Big Bird').

Based on this sky map, we compared our model neutrino spectra from the Wd1 source with the fluxes in five IceCube energy bins corresponding to the five neutrinos within 2σ of the source. This is shown in the Fig. 5. A more precise comparison will require both more sophisticated models of the cloud distribution within a few hundred parsecs of Wd1 and a more accurate determination of the event positions.

5 DISCUSSION

Explaining the origin of the recently detected PeV neutrinos by IceCube is a fundamental challenge for models of particle acceleration. The observations imply a source that can produce substantial fluxes of protons with energies considerably higher than those expected from isolated SNRs. Since isolated SNRs remain the most likely source of CRs below a few PeV, the neutrino source must produce high-energy protons without conflicting with the observed properties of galactic CRs. The underlying protons producing the neutrinos in the CSF model described above have a hard spectrum, and are few in number, avoiding any conflict with low-energy CR population measurements. The CSFs may contribute to the high-energy end of the CR population produced by isolated SNRs and superbubbles (see e.g. Binns et al. 2007) and, we believe the strong plasma flows in compact clusters of young stars, such as Wd1, contain the energy and specific properties needed to explain a significant fraction of the IceCube neutrinos.

Compact clusters contain massive stars with strong winds and recent SN activity. It is inevitable that occasions will occur when an SN blast wave collides with the termination shock from the strong wind of a nearby massive star, or with an extended cluster wind from several massive stars. We have developed a model of the *Fermi* acceleration expected from such CSFs and, using realistic parameters, obtained simultaneous fits to the H.E.S.S. gamma-ray observations (Fig. 4) and the fraction of IceCube neutrinos expected from Wd1 (Fig. 5).

5.1 Multiwavelength signatures of CSF scenario

A unique property of our CSF model is that the acceleration, while producing hard proton spectra to multi-PeV energies with high efficiencies, only lasts a small fraction of the SNR lifetime, just the time when the SNR is colliding with the nearby stellar wind. Because of the hard spectra of accelerated CRs most of the energy is in the highest energy regime. In Fig. 3, we show the predictions for high-energy photon and neutrino emission of the source at the end of the acceleration stage (which was supposedly $\sim 10^4$ yr ago). The synchrotron radio emission then is estimated to be $\gtrsim$10 Jy at 2.2 GHz, a value well above the current level. This is consistent with our scenario where the brief CR acceleration stage ended $\sim 10^4$ yr ago.

Indeed, the total radio flux from Wd1 as measured with the *Australia Telescope Compact Array* (ATCA) interferometer by Dougherty et al. (2010) is 422, 461, 523, and 669 mJy at 8.6, 4.8, 2.2, and 1.4 GHz, respectively, and after subtracting the radio emission from stellar sources, they derived diffuse emission fluxes of 307, 351, and 426 mJy at 8.6, 4.8, and 2.2 GHz. Colliding winds in massive binary star systems were proposed by Eichler & Usov (1993) to accelerate relativistic particles and produce non-thermal radio and GeV regime gamma-ray emission. Some of the stellar radio sources detected in Wd1 with the ATCA by Dougherty et al. (2010) exhibited composite spectra of both non-thermal and thermal emission potentially indicating particle acceleration in colliding wind binaries.

In contrast to the binary wind model, CRs in CSFs are generated in the violent environment of an SN blast wave colliding with a cluster wind. While the acceleration stage is brief, CRs will escape the source and interact with the nearby ISM clouds for long periods ($\gtrsim 10^4$ yr). During this time pions will be produced in inelastic p–p-interactions resulting in relativistic secondary electrons and positrons from $\pi^\pm$ decay and photons from π^0 decay. The hard CR spectra from CSFs will result in prominent peaks in the spectral energy distribution produced by synchrotron, IC, and pion-decay emission, as shown in Fig. 7. For an extended cloud of size $\sim$30 pc and number density $\sim$25 cm^{-3}, the peaks correspond to keV, TeV, and PeV energy bands.

For Fig. 7 we assumed the cloud magnetic field to be $B = 10$ μG consistent with Zeeman splitting measurements of a number of

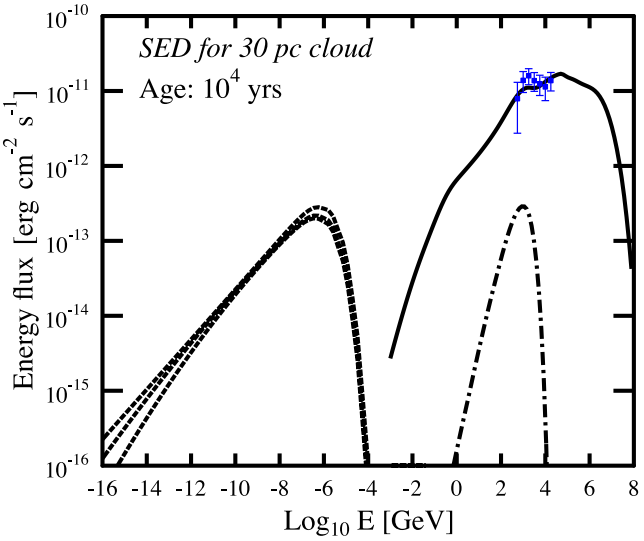

Figure 7. The spectral energy distribution of the synchrotron (dashed lines), IC (dot–dashed line) emission from secondary electrons and positrons, as well as photons produced by pion-decay (solid line) from the inelastic p–p-interactions in the nearby clouds which are H.E.S.S. sources shown in Fig. 2. The CRs were accelerated at Wd1 and diffused into the clouds. The cloud gas number density is 25 cm^{-3} with magnetic field $B = 10$ μG. The gamma-rays detected by H.E.S.S. are indicated in the figure. The upper dashed synchrotron curve is the result with no energy threshold for CR protons to penetrade into the cloud. The lower synchrotron curves correspond to threshold values 10 GeV and 20 GeV, respectively. The threshold values are low enough to not influence the pion-decay emission.

molecular clouds compiled recently by Strong et al. (2014). Since the penetration of CR nuclei into the cloud may be reduced at low energies (e.g. Cesarsky & Volk 1978; Protheroe et al. 2008), we show in Fig. 7 spectra for the case with no proton penetration energy threshold (upper dashed curve) and for proton threshold energies $E_* = 10$ and 20 GeV. The radio fluxes are sensitive to E_* but the X-ray synchrotron fluxes corresponding to the peak of the synchrotron SED are not.

The cloud associated with the H.E.S.S. source in this model is a diffuse, low-surface-brightness ($\lesssim$0.1 μJy arcsec^{-2} at 1.4 GHz), flat-spectrum, synchrotron source of polarized radio emission with bright spots of brightness ∼1 mJy arcsec^{-2} at 1.4 GHz, corresponding to local strong enhancements of the magnetic field in dense clumps. The future Square Kilometre Array, with a sensitivity of ∼1 μJy beam^{-1}, may allow detection of radio emission from clouds irradiated by CRs (see e.g. Strong et al. 2014).

The synchrotron peak in the CSF model is at keV X-ray energies and a source with a half-degree extension and total flux of ∼10^{-13} erg cm^{-2} s^{-1} may be detectable with the future eROSITA (extended ROentgen Survey with an Imaging Telescope Array) instrument on the *Spectrum-Roentgen-Gamma* satellite (see e.g. Cappelluti 2011). The search for synchrotron X-ray emission from the cold clouds located near these powerful CR sources may be conducted with the next generation of X-ray sky surveys.

In Fig. 4, we show simulated spectra of gamma-ray emission from CRs that escaped the accelerator and diffused into the surrounding cloudy medium over 10^4 yr. The models are compared to H.E.S.S. data for the source associated with Wd1 (Abramowski et al. 2012a; Ohm et al. 2013) and we have reduced the gamma-ray flux to correspond to the H.E.S.S. field of view at Wd1. At 10^4 yr, the acceleration responsible for the emission has long ceased and the emission comes only from CRs accelerated in the source and propagating through the ISM.

We note that an analysis of 4.5 yr of *Fermi-LAT* data by Ohm et al. (2013) found extended emission offset from Wd1 by about 1°. This study concluded that acceleration of electrons in a pulsar wind nebula could provide a natural explanation of the observed GeV emission. However, Ohm et al. (2013) found that the pulsar wind nebula could not explain the TeV emission observed by H.E.S.S.As seen in Fig. 4, the CSF model can satisfactorily explain the TeV gamma-ray emission.

There is an apparent excess of neutrino events, including two of the three PeV neutrinos in the IceCube map presented in Aartsen et al. (2014a), within a radian from Wd1. In Fig. 6, we show this set in a map with the positions of the events and 2σ contours as determined from 2D Gaussian statistics and the median angular errors of the IceCube telescope. Wd1 is indicated with a contour (black circle) corresponding to a 140 pc radius region – a few degrees – where neutrinos are produced in our CSF model as escaping CRs diffuse out from the compact accelerator for ∼10^4 yr. The neutrino energy flux corresponding to the solid curve in Fig. 5 is ∼3.7 × 10^{-8} GeV cm^{-2} s^{-1}. This is well below the 90 per cent confidence level upper limits imposed by ANTARES observations (Adrián-Martínez et al. 2014) for a source of width >0.°5 degrees at the Wd1 declination.

5.2 CSFs in the starburst galaxies

Another issue concerns how hard spectrum PeV neutrino sources contribute to starburst galaxy radiation. The population of star-forming galaxies with AGNs and the starburst galaxies peaked at a redshift $z \gtrsim 1$, with a wide tail of the distribution revealed by *Herschel* (Gruppioni et al. 2013) up to $z \sim 4.5$. These objects most likely contribute to both the isotropic diffuse gamma-ray background measured by *Fermi-LAT* (Ackermann et al. 2015) between 100 MeV and 820 GeV, and the diffuse flux of high-energy neutrinos measured by IceCube.

Assuming that a CR spectral index for all the starburst-like galaxies is 2.1–2.2 at the high-energy part of the spectrum, Tamborra et al. (2014) were able to provide a reasonable fit to both the *Fermi* and IceCube data. Larger indices failed to explain the observed diffuse neutrino flux. That CR spectra harder than in normal galaxies like the Milky Way were required, may reflect a different population of CR sources and/or different CR propagation in the starburst galaxies. Superclusters of young massive stars are likely much more abundant in starburst galaxies compared to the Milky Way since mergers and interactions of galaxies result in abundant supercluster formation (see e.g. Conti, Crowther & Leitherer 2012). The hard spectra and high efficiencies from CSFs make them an attractive way to produce CRs well beyond PeV in starburst galaxies where the collective contribution from many CSFs sources might extend the CR knee to higher energies compared to the Milky Way.

High-resolution radio observations of the star-forming galaxies M82, Arp 220, NGC 253, M31, M33 and others provide information on the magnetic field structure and leptonic CRs (Adebahr et al. 2013; Tabatabaei et al. 2013; Persic & Rephaeli 2014), and gamma-ray telescopes have observed some starburst galaxies up to ∼10 TeV (see Acero et al. 2009; Lacki et al. 2011; Abramowski et al. 2012b; Ackermann et al. 2012, and the references therein). However, this is still well below PeV energies, where CSF CRs are expected to be dominant and the *Cherenkov Telescope Array* (Actis et al. 2011) would be needed to constrain the gamma-ray spectra in PeV energy regime. More quantitative models of the CSF contribution

to the diffuse gamma-ray and neutrino backgrounds will require better statistics of CSF SNe in starburst regions, accurate models of CR escape from the sources, as well as realistic models of CR propagation in starburst regions.

6 CONCLUSIONS

We have presented a CSF model for CR production in compact stellar clusters that efficiently produces hard CR spectra and neutrinos. Acceleration in colliding plasmas is a very efficient version of *Fermi* acceleration given the strong confinement of CRs in the converging flows. The mechanism is strongly non-linear and time-dependent. We simulated the acceleration process in a simplified geometry. Protons escape the accelerator with varying hardness and maximum energy as the SN shock approaches the wind. Furthermore, there is uncertainty in details of the mass distribution in the complicated outer ISM region (e.g. dense clouds) which will influence the results. Nevertheless, we believe our simulations include enough essential physics to estimate the neutrino and gamma-ray emission from the galactic cluster Wd1 and we show it is a likely source for IceCube events detected from the inner galaxy. Our gamma-ray predictions are consistent with H.E.S.S observations as well.

While the relatively large angular uncertainty in the arrival directions of PeV neutrinos precludes an exact identification, we believe some PeV IceCube events may result from $\geq$10 PeV CR protons accelerated in Wd1 (see Fig. 6). This cluster is a good candidate because it is one of the most massive clusters in the Local Group of galaxies and has an observed 10^4 yr old magnetar, allowing enough time to spread PeV CRs over a few hundred parsec scale.

Future work that is critical for determining if a galactic supercluster can explain the apparent clump of 4–5 IceCube events includes developing a more accurate model of multi-PeV CR diffusion on kpc scales. This requires a careful treatment of the matter distribution within a few degrees of Wd1 and will result in a more accurate determination of the neutrino flux, as well as radio to gamma-ray emission, from CR interactions.

ACKNOWLEDGEMENTS

We thank the anonymous referee for careful reading of our paper and useful comments. AMB thanks Markus Ackermann for a useful discussion. DCE acknowledges support from NASA grant NNX11AE03G. DCE wishes to thank the International Space Science Institute (ISSI) in Bern where part of this work was done.

REFERENCES

Aartsen M. G. et al., 2014a, Phys. Rev. Lett., 113, 101101
Aartsen M. G. et al., 2014b, ApJ, 796, 109
Abramowski A. et al., 2012a, A&A, 537, A114
Abramowski A. et al., 2012b, ApJ, 757, 158
Acero F. et al., 2009, Science, 326, 1080
Acero F., Lemoine-Goumard M., Renaud M., Ballet J., Hewitt J. W., Rousseau R., Tanaka T., 2015, preprint (arXiv:1506.02307)
Ackermann M. et al., 2012, ApJ, 755, 164
Ackermann M. et al., 2015, ApJ, 799, 86
Actis M. et al., 2011, Exp. Astron., 32, 193
Adebahr B., Krause M., Klein U., Weżgowiec M., Bomans D. J., Dettmar R.-J., 2013, A&A, 555, A23
Adrián-Martínez S. et al., 2014, ApJ, 786, L5
Aharonian F. A., 2004, Very High Energy Cosmic Gamma Radiation: A Crucial Window on the Extreme Universe. World Scientific Press, Singapore
Aharonian F. A., 2013, Astropart. Phys., 43, 71
Ahlers M., Murase K., 2014, Phys. Rev. D, 90, 023010
Amato E., 2014, Int. J. Mod. Phys. D, 23, 30013
Anchordoqui L. A. et al., 2014a, J. High Energy Astrophys., 1, 1
Anchordoqui L. A., Paul T. C., da Silva L. H. M., Torres D. F., Vlcek B. J., 2014b, Phys. Rev. D, 89, 127304
Becker J. K., 2008, Phys. Rep., 458, 173
Bell A. R., 2004, MNRAS, 353, 550
Binns W. R. et al., 2007, Space Sci. Rev., 130, 439
Blandford R., Simeon P., Yuan Y., 2014, Nucl. Phys. B, 256, 9
Blasi P., 2013, A&AR, 21, 70
Budnik R., Katz B., MacFadyen A., Waxman E., 2008, ApJ, 673, 928
Bykov A. M., 2014, A&AR, 22, 77
Bykov A. M., Gladilin P. E., Osipov S. M., 2011, Mem. Ital. Astron. Soc., 82, 800
Bykov A. M., Gladilin P. E., Osipov S. M., 2013, MNRAS, 429, 2755
Bykov A. M., Ellison D. C., Osipov S. M., Vladimirov A. E., 2014, ApJ, 789, 137
Cappelluti N., 2011, Mem. Soc. Astron.. Ital. Suppl., 17, 159
Cesarsky C. J., Volk H. J., 1978, A&A, 70, 367
Chakraborti S., Ray A., Soderberg A. M., Loeb A., Chandra P., 2011, Nature Commun., 2
Chevalier R. A., Clegg A. W., 1985, Nature, 317, 44
Clark J. S., Negueruela I., Crowther P. A., Goodwin S. P., 2005, A&A, 434, 949
Conti P. S., Crowther P. A., Leitherer C., 2012, From Luminous Hot Stars to Starburst Galaxies. Cambridge Univ. Press, Cambridge
Crowther P. A., Hadfield L. J., Clark J. S., Negueruela I., Vacca W. D., 2006, MNRAS, 372, 1407
Dougherty S. M., Clark J. S., Negueruela I., Johnson T., Chapman J. M., 2010, A&A, 511, A58
Dwek E., Krennrich F., 2013, Astropart. Phys., 43, 112
Earl J. A., 1974, ApJ, 188, 379
Eichler D., Usov V., 1993, ApJ, 402, 271
Fox D. B., Kashiyama K., Mészarós P., 2013, ApJ, 774, 74
Gieles M., Portegies Zwart S. F., 2011, MNRAS, 410, L6
Gruppioni C. et al., 2013, MNRAS, 432, 23
Halzen F., 2013, Astropart. Phys., 43, 155
Halzen F., Hooper D., 2002, Rep. Prog. Phys., 65, 1025
He H.-N., Yang R.-Z., Fan Y.-Z., Wei D.-M., 2013, preprint (arXiv:1307.1450)
Kafexhiu E., Aharonian F., Taylor A. M., Vila G. S., 2014, Phys. Rev. D, 90, 123014
Kashiyama K., Mészáros P., 2014, ApJ, 790, L14
Kashiyama K., Murase K., Horiuchi S., Gao S., Mészáros P., 2013, ApJ, 769, L6
Kelner S. R., Aharonian F. A., Bugayov V. V., 2006, Phys. Rev. D, 74, 034018
Lacki B. C., Thompson T. A., Quataert E., Loeb A., Waxman E., 2011, ApJ, 734, 107
Liu R.-Y., Wang X.-Y., Inoue S., Crocker R., Aharonian F., 2014, Phys. Rev. D, 89, 083004
Mereghetti S., 2008, A&AR, 15, 225
Mészáros P., Waxman E., 2001, Phys. Rev. Lett., 87, 171102
Muno M. P. et al., 2006a, ApJ, 636, L41
Muno M. P., Law C., Clark J. S., Dougherty S. M., de Grijs R., Portegies Zwart S., Yusef-Zadeh F., 2006b, ApJ, 650, 203
Murase K., Ahlers M., Lacki B. C., 2013, Phys. Rev. D, 88, 121301
Neronov A., Semikoz D., Tchernin C., 2014, Phys. Rev. D, 89, 103002
Ohm S., Hinton J. A., White R., 2013, MNRAS, 434, 2289
Persic M., Rephaeli Y., 2014, A&A, 567, A101
Protheroe R. J., Ott J., Ekers R. D., Jones D. I., Crocker R. M., 2008, MNRAS, 390, 683
Ptuskin V., Zirakashvili V., Seo E.-S., 2010, ApJ, 718, 31

Razzaque S., 2013, Phys. Rev. D, 88, 081302
Schure K. M., Bell A. R., O'C Drury L., Bykov A. M., 2012, Space Sci. Rev., 173, 491
Stecker F. W., 2013, Phys. Rev. D, 88, 047301
Stevens I. R., Hartwell J. M., 2003, MNRAS, 339, 280
Strong A. W., Moskalenko I., Ptuskin V. S., 2007, Annu. Rev. Nucl. Part. Sci., 57, 285
Strong A. W., Dickinson C., Murphy E. J., 2014, preprint (arXiv:1412.4500)
Tabatabaei F. S., Berkhuijsen E. M., Frick P., Beck R., Schinnerer E., 2013, A&A, 557, A129
Tamborra I., Ando S., Murase K., 2014, J. Cosmol. Astropart. Phys., 2014, 043
Waxman E., Bahcall J., 1997, Phys. Rev. Lett., 78, 2292
Wilkin F. P., 1996, ApJ, 459, L31
Wright N. J., Parker R. J., Goodwin S. P., Drake J. J., 2014, MNRAS, 438, 639

This paper has been typeset from a TEX/LATEX file prepared by the author.